Tuijin Jishu/Journal of Propulsion Technology
ISSN: 1001-4055
Vol. 45 No. 3 (2024)

# Evaluating Mechanical Behavior of PLA Under Varied Strain Rates Using Stereolithography 3D Print Method

**B. Dwinata[1], B. Budiwantoro[2], A. Wibowo[3], M. A. Kariem[4]**
[1] *Universitas Jenderal Achmad Yani*
[2, 3, 4] *Institut Teknologi Bandung*

***Abstract:-*** Poly-L-lactic acid (PLA), a type of aliphatic polyester, has garnered significant attention in recent years due to its favorable mechanical properties, biocompatibility, and biodegradability. Derived from renewable resources such as corn starch and sugarcane, PLA is a sustainable alternative to petroleum-based plastics, aligning with global efforts to reduce environmental impact. The resin's ability to degrade into non-toxic lactic acid in biological environments makes it particularly suitable for medical applications, including sutures, drug delivery systems, and orthopedic implants. Focus of this study is evaluation of the comparative mechanical properties of PLA at varied low strain rates (quasi-static) through tensile and compression testing. The aims of this study are analyzing the strain rate sensitivity of PLA, defining the constitutive model of PLA, validating the viscoelastic constitutive model for PLA by comparing the experimentally tested mechanical response with the constitutive model. ASTM D695.6642 was applied for compressive testing with varied strain rate 10-3 s-1 and 10-4 s-1, resulted the difference of average Young's Modulus and average yield stress 18.81% and 19.88% respectively. ASTM-D638-03 was applied for tensile testing, showed the difference of Young's Modulus and yield stress 9.76% and 43.82% respectively. Simplified Zhu – Wang – Tang constitutive model was derived from the experimental data, resulted the R2 value 0.993 in elastic region. Lastly, the Mohr – Coulomb failure criterion was applied to define the failure between compressive and tensile behavior.

***Keywords****:* PLA, constitutive model, Simplified Zhu – Wang – Tang, Mohr – Coulomb criteria.

## 1. Introduction

Poly-L-lactic acid (PLA) is an aliphatic polyester known for its biodegradability and biocompatibility, making it highly attractive for numerous applications, especially in the medical field. Produced from renewable sources such as corn starch and sugarcane, PLA supports global efforts towards sustainability and eco-friendliness (Niaounakis, 2015). Its capability to break down into non-toxic lactic acid within biological environments positions it as a prime material for biomedical uses, including sutures, drug delivery systems, and notably, bone implants (DeStefano et al., 2020; Sreekumar et al., 2021). PLA's biocompatibility and biodegradability ensure that the implants are safe and gradually resorb into the body, eliminating the need for surgical removal. Additionally, the mechanical properties of PLA, such as its tensile strength and modulus, can be engineered to mimic those of natural bone by incorporating fillers like hydroxyapatite (HA) . Unlike the metallic or ceramic based bone implants which are significantly stiffer than human bone, leading to the phenomenon of stress shielding. This stress shielding effect results the reduction in bone density around the implant. (Raffa et al., 2021). Several studies have highlighted the drawbacks of metal-based bone implants, particularly their potential to release toxic metal ions during body imaging processes such as CT scans or MRI scans (Han et al., 2019). In other hand, ceramic-based bone implants, while biocompatible, are brittle and have low fracture resistance (Ma and Tang, 2014). PLA based composite implant material not only enhances the mechanical performance of the implants but also promotes bone ingrowth and integration due to HA's osteoconductive properties (Islam et al., 2020; Wang et al., 2021; Zhang et al., 2021).

In recent years, the advancement of additive manufacturing technologies, especially 3D printing, has revolutionized the fabrication of complex structures with high precision and customization capabilities. Studies by W. Wang et al. and Zhou C. et al. have characterized nano HA + PLA bone implants using 3D printing Fused Deposition Modelling (FDM). Mechanical evaluation was conducted by testing the compressive strength of the specimens quasi-statically and the biological evaluation was done by assessing osteogenesis and biocompatibility both in vitro and in vivo (Wang et al., 2021; Zhang et al., 2021; Zhou et al., 2021). The 3D printing FDM method is commonly used for extracting HA + PLA bone implant specimens (Esmaeili et al., 2020; Hassanajili et al., 2019; Ranjan et al., 2020; Wu et al., 2020). Although this FDM method considerably cost effective, this method has several limitations, such as low geometrical accuracy, rough surface finish, anisotropic mechanical property, To overcome those limitations, Stereolithography (SLA) method stands out for its ability to produce high-resolution objects with intricate details. SLA uses a photopolymerization process where a laser cures liquid resin layer by layer to form solid structures. This method's precision is particularly beneficial for creating customized medical implants that require exact geometries and fine details (Gide et al., 2022).

Recent research on HA + PLA composite material testing primarily provides data on quasi-static compression testing with the single strain rate value around $10^{-4}$ $s^{-1}$ of. However, most physiological bone fractures are associated with much higher strain rates. For instance, in vivo loading rate measurements on bones indicate strain rates of approximately 0.007 to 0.013 $s^{-1}$, during walking or running, and up to 0.02 $s^{-1}$, during sprinting, downhill, and any other swift activities, the upper limit for high strain rates can reach around 25 $s^{-1}$ (Zimmermann et al., 2014). Another study highlights that the intermediate strain rate range of 1-100 $s^{-1}$ represents the region where many dynamic bone fractures occur (Cloete et al., 2014). These kind of dynamic span value of strain rates needs to be evaluated due to the mechanical behavior. Research on cancellous bone testing with varying strain rates has demonstrated that the mechanical properties of cancellous bone are strain rate sensitive (Prot et al., 2016). The testing involved comparing the maximum axial stress parameters across different strain rate classifications: low strain rate (quasi-static 0.001/s to 0.1/s), intermediate strain rate (wedge bar 1/s to 100/s), and high strain rate (Split Hopkinson Pressure Bar 400/s to 600/s). This comprehensive analysis provides valuable insights into how cancellous bone responds under different loading conditions, highlighting the importance of strain rate in determining its mechanical behavior. Other study of strain rate sensitivity on polymer fabricated by SLA method reported that the samples have significantly different mechanical behavior under varied strain rate (Sælen et al., 2023).

Given the realistic physiological conditions represent strain rates that are approximately four times higher or more than those used in most laboratory fracture experiments, also the mechanical behavior of cancellous bone or polymer which fabricated by SLA method, it is crucial to characterize and understand the role of strain rates in influencing the multi-scale mechanisms employed by PLA based polymer as bone implant to resist fractures. This study aims to evaluate mechanical behavior of PLA resin fabricated by SLA method under varied strain rates and to evaluate the compression over the tension material respond. There are two expected result of this study:

1. To generate the constitutive model of material, this constitutive model should capture the different strain rate effect of PLA.
2. To generate the failure criterion model of material, this failure criterion should explain if there is the significant difference between compression and tension test result.

## 2. Materials and Methods

### 2.1 SLA 3D Printing

The resin used in this study is eResin-PLA, a type of Bio-photopolymer Resin manufactured by ESUN. This resin contains a photoinitiator to facilitate the SLA 3D printing process. It possesses good toughness, excellent surface finish, and is certified with the EN71-3 standard, ensuring safety regarding the migration of certain chemicals into the body if ingested. The preparation for the SLA 3D printing process begins by designing the sample geometry in .stl format. The .stl file is then processed using slicing software such as CHITUBOX, which performs several key functions:

1. Visualizing the part to be printed according to the geometric capacity of the selected 3D printer.
2. Planning the 3D printing process with specific coordinates and part orientation.
3. Selecting the type and location of supports.
4. Setting printer parameters such as exposure time, layer height, lift distance, lift speed, retract distance, and retract speed.
5. Slicing the model to generate G-code for laser movement on each layer.
6. Transferring the file via flash drive for use in the 3D printer.

Machine Parameters and Post-Processing

The 3D printing process was carried out on a Phrozen Mighty 8K machine, which includes a curing unit. The Phrozen Mighty 8K 3D printer offers a notable advantage with its XY axis resolution of 28 µm. This high resolution allows for the generation of samples with superior geometric accuracy compared to the fused deposition modeling (FDM) method.

The parameters of the 3D printer need to be adjusted based on the type of resin used to produce a product with good geometry and an optimal process duration. For bio-photopolymer resin, the recommended parameters are: exposure time of 4.2 seconds, layer height of 0.05 mm, lift distance of 8 mm, retract distance of 8 mm, lift speed of 60 mm/min, and retract speed of 150 mm/min.Once the 3D printing process is complete, the sample is cleaned with alcohol to ensure it is free from contaminants or residual resin fluids. Subsequently, the curing process is carried out to ensure the resin is properly solidified.

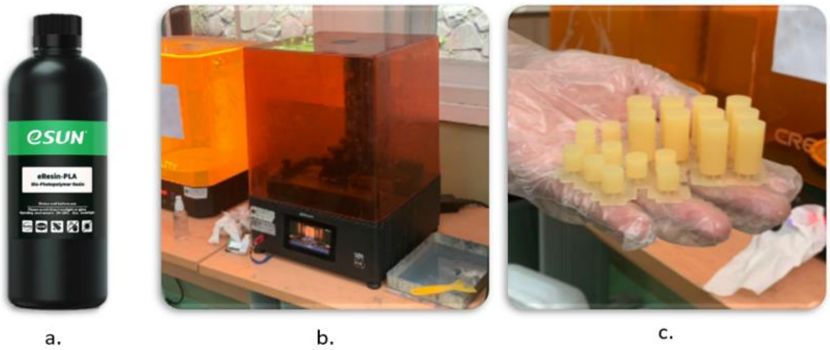

**Fig. 1. a. e-Resin PLA Bio-photopolymer by ESUN; b. 3D Print SLA process; c. PLA samples of 3D Print SLA**

### 2.2 Mechanical Testing

Experimental tests of polymer-based bone implant samples were carried out in two main stages. The first stage is experimental tests with $10^{-4}$ $s^{-1}$ strain rate and the second stage is experimental tests with $10^{-3}$ $s^{-1}$ strain rate. The tests were conducted by considering the tensile and compressive strength of the samples. Experimental testing with a low strain rate is in the form of compressive testing of PLA samples by applying the ASTM D695-15 standard on "Standard Test Method for Compressive Properties of Rigid Plastics". Meanwhile, ASTM D 638-03 "Standard Test Method for Tensile Properties of Plastics" was used to determine the mechanical properties in the form of tensile strength of the samples.

The testing machine used was the INSTRON 5985 Universal Testing Machine. This device is used for both tensile and compressive testing. INSTRON 5985 has a maximum load capacity of 250 kN. The machine is equipped with a double column frame designed to reduce deflection during application of high loads, thus ensuring accuracy and consistency of test results. The machine utilizes a servo-hydraulic or servo-electric drive system. A digital control system can be applied to set test parameters, monitor the test process in real-time, and collect data with high accuracy. Bluehill® Universal software is often used to control the machine and analyze data.

The compression experimental test is used to examine the mechanical properties of PLA with compression loading at a constant strain rate. The parameter produced in this test is the force to elongation curve of the specimen. Next, These values are then being processed into a stress to strain curve either in the engineering stress - strain state, or true stress – strain. The geometry of compressive test specimen is cylindrical with 12.7 mm diameter and 25.4 mm length. In tensile testing, a Digital Image Correlation (DIC) module is used to calculate the Poisson's Ratio of the sample. The device consists of a camera equipped with infrared light. Initially, the sample is marked in the axial and lateral directions, and then the DIC module can predict the movement or deformation of the markings in the axial and lateral directions defined as axial strain and lateral strain. The ratio between lateral and axial strain is defined as Poisson's Ratio. The tensile test sample has a total length of 165 mm, with a gage length of 57 mm, and a thickness of 3.2 mm.

The tests used the same 3 samples for each strain rate category. Tests were conducted with different strain rates, including: $\dot{\varepsilon_1} = 10^{-3}s^{-1}10$ and $\dot{\varepsilon_2} = 10^{-4}s^{-1}$. To achieve these test conditions, we need to adjust the testing speed on the machine (v), where the relationship between the strain rate and the machine speed is shown in the following equation:

$$v\left(\frac{mm}{min}\right) = \dot{\varepsilon}\left(\frac{1}{s}\right) \times L(mm) \times 60\left(\frac{s}{min}\right) \qquad (1)$$

Where L is the length of the specimen in the compressive test or gage length in the tensile test. We adjusted the testing speed to analyze the sensitivity of the sample strength to different strain rates. In addition, this test is also important for parameter input for constitutive modeling of viscoelastic materials.

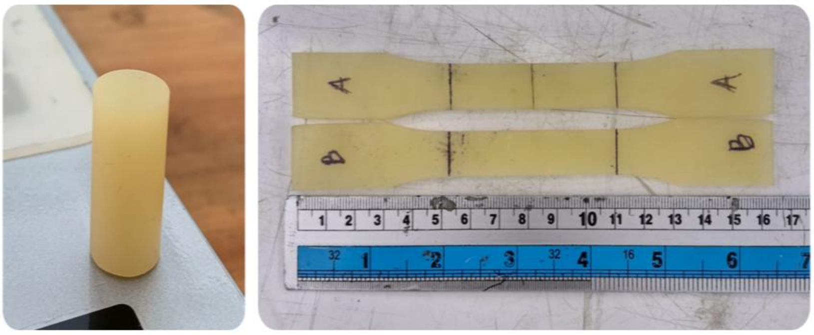

a. b.

**Fig. 2. a. Compressive test sample; b. Tensile test sample**

## 2.3 Statistical Analysis

Statistical Analysis was conducted using R Studio software (Boston, USA). The result of the test is presented in boxplot which serve the data of mean and standard deviation. Statistical T test was used to assess the homogeneity of variances. The results were considered significant if $p < 0.05$. The Levenberg-Marquardt algorithm was used for the approximation of PLA constitutive model. This algorithm was used for numerical optimization used to solve curve fitting problems in non-linear models. It is an iterative algorithm that combines two different approaches: the Gauss – Newton method and the stochastic gradient method.

## 2.4 Data Processing

### 2.4.1 Stress vs Strain Curves

The raw information form compressive or tensile test is force to displacement data. This force and displacement data can be processed into engineering stress to engineering strain, by applying the equations below:

$$\sigma_E = \frac{F}{A} \quad dan \quad \varepsilon_E = \frac{\Delta L}{L_0} \qquad (2)$$

Where $\sigma_E$ indicates engineering stress (MPa); $\varepsilon_E$ indicates engineering strain; F indicates force (N); A indicates cross sectional area (mm$^2$); $\Delta L$ indicates displacement (mm); and $L_0$ indicates initial length of the sample (mm). From the engineering stress to engineering strain curve, we can gather Young's Modulus by calculating the slope of the curve in elastic region, and yield stress by selecting the point along the curve where there is tend to be not linear anymore. Next, the true stress and true strain curve can be gathered by applying the equations below:

$$\sigma_{tr} = \sigma_E(1 + \varepsilon_E) \quad dan \quad \varepsilon_{tr} = \ln(1 + \varepsilon_E) \ (3)$$

Where $\sigma_{tr}$ indicates true stress (MPa); $\varepsilon_{tr}$ indicates true strain.

Poisson's Ratio measurement was done by comparing lateral strain and longitudinal strain. Samples were marked longitudinally and laterally first, then the markers were scanned by a Digital Image Correlation (DIC) device. The Poisson's Ratio calculation applies the comparison of lateral and longitudinal strains in the elastic phase.

### 2.4.2 Simplified Zhu – Wang – Tang Constitutive Model

The phenomenon of mechanical behavior difference under varied strain rates was modeled as the Simplified Zhu - Wang – Tang (ZWT) constitutive model. This constitutive model is a mathematical equation that predicts the stress - strain curve of a sensitive material to the loading rate. The limitation of this model is only predicting the material properties in the elastic phase. It was reported in several studies that modeling polymer-based materials with the Zhu-Wang-Tang model has a very low deviation or error value (Gao et al., 2024; Ji et al., 2021; Xu et al., 2018). The author tries to adapt the Zhu - Wang - Tang model by simplifying the model to be simpler where the strain rate range is only limited to the psychological loading conditions of the bone ($10^{-4}$ $s^{-1}$ – 25 $s^{-1}$).

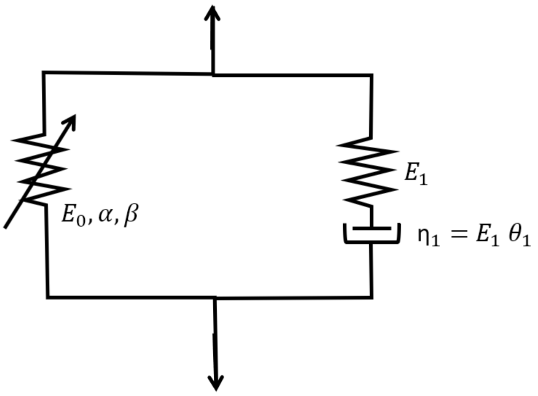

**Fig. 3.The rheological model of Simplified Zhu – Wang – Tang material constitutive model.**

The Simplified ZWT viscoelastic model consists of element 0 which models a nonlinear spring, element I which models Maxwell's viscoelastic properties with a low strain rate. The following are the equations of the Simplified ZWT constitutive model:

$$\sigma = E_0\varepsilon + \alpha\varepsilon^2 + \beta\varepsilon^3 + E_1\int_0^t \dot{\varepsilon} exp\left(-\frac{t-\tau}{\theta_1}\right)d\tau \qquad (4)$$

Where $E_0$, $\alpha$, and $\beta$ are nonlinear elastic constants, $E_1$ and $\theta_1$ are elastic constants and relaxation time at low strain rate of Maxwell's I element model, and the viscosity coefficient is $\eta_1 = E_1\theta_1$. The first step is defining the equation for the difference in stress values between the two states of strain rates ($10^{-3}$ $s^{-1}$ and $10^{-4}$ $s^{-1}$) which can be written as the following equation:

$$\Delta\sigma = \sigma_1 - \sigma_2 \qquad (5)$$

Where $\sigma_1$ is the true stress value of compression test under $10^{-3}$ $s^{-1}$ strain rate value; $\sigma_2$ is the true stress value of compression test under $10^{-4}$ $s^{-1}$ strain rate value. The second step is curve fitting the $\Delta\sigma$ to strain curve with the Eq. 6 to define $E_1$ and $\theta_1$ coefficient value. The curve fitting process was performed with R studio software with the nlsLM() function. This function applies the Levenberg-Marquardt algorithm used for numerical optimization used to solve curve fitting problems in non-linear models.

$$\Delta\sigma = E_1 \int_0^{\frac{\varepsilon}{\dot{\varepsilon_1}}} \dot{\varepsilon_1} exp\left(-\frac{\frac{\varepsilon}{\dot{\varepsilon_1}} - \tau}{\theta_1}\right) d\tau - E_1 \int_0^{\frac{\varepsilon}{\dot{\varepsilon_2}}} \dot{\varepsilon_2} exp\left(-\frac{\frac{\varepsilon}{\dot{\varepsilon_2}} - \tau}{\theta_1}\right) d\tau$$

$$= E_1\theta_1\dot{\varepsilon_1}\left(1 - \exp\left(-\frac{\varepsilon}{\dot{\varepsilon_1}\theta_1}\right)\right) - E_1\theta_1\dot{\varepsilon_2}\left(1 - \exp\left(-\frac{\varepsilon}{\dot{\varepsilon_2}\theta_1}\right)\right) \quad (6)$$

The third step is gathering quasi static parameters $E_0$, $\alpha$ and $\beta$ by doing the second curve fitting process. This can be done by matching one of the compression test true stress and true strain result with the Eq. 4. Finaly all of the coefficients $E_0$, $\alpha$, $\beta$, $E_1$ and $\theta_1$ have been defined. Note that all of the curve fitting processes, the value of $R^2$ has to be greater than 0.9.

### 2.4.3 Mohr – Coulomb Failure Criteria

The phenomenon of different mechanical parameters due to different types of loading between tensile and compressive is modeled by the Mohr - Coulomb failure criteria model.

This failure criteria model is one of the models that describes the difference in yield strength of a material when loaded with tensile load or compression load. The failure region can be described with the tangent line of compressive loading Mohr's circle and the tensile loading Mohr's circle. The area outside the line is considered as failure region.

In addition to Mohr diagram analysis, the Mohr - Coulomb failure criteria model can also predict material failure through the Plane Stress Yield Surface of pure PLA material. If the stress planes are applied loads $\sigma_A$ and $\sigma_B$,The mathematical equation for the Mohr – Coulomb failure criterion model is as follows:

$$\frac{\sigma_1}{\sigma_{y,t}} - \frac{\sigma_3}{\sigma_{y,c}} \leq 1 \qquad (7)$$

Where $\sigma_1$ is the largest tri-axial stress component (MPa); $\sigma_3$ is the least tri-axial stress component (MPa); $\sigma_{y,t}$ is the tensile yield strength (MPa); $\sigma_{y,c}$ is the compressive yield strength (MPa).

## 3. Results

### 3.1 Experimental Test Results

#### 3.1.1 Compressive Test Resul

Tests were conducted on 6 samples where the initial 3 samples were tested at a strain rate of $10^{-3}$ $s^{-1}$ while the next 3 samples were tested at a strain rate of $10^{-4}$ $s^{-1}$. The test resulting the force and displacement information that can be processed into engineering stress and engineering strain curve, as well as true stress and true strain curve through the Eq. 2 and 3 respectively.

From this information, several mechanical parameters can be obtained, which are listed in the table 1 below:

**Tabel 1: Extraction of compression test parameters**

| Label | Strain Rate ($s^{-1}$) | Young's Modulus (GPa) | Compressive Yield Stress (MPa) |
|---|---|---|---|
| c_high1 | $10^{-3}$ | 1.36 | 59.26 |
| c_high2 | $10^{-3}$ | 1.22 | 59.97 |
| c_high3 | $10^{-3}$ | 1.30 | 58.71 |
| c_low1 | $10^{-4}$ | 1.13 | 51.34 |
| c_low2 | $10^{-4}$ | 1.09 | 48.96 |
| c_low3 | $10^{-4}$ | 1.05 | 48.13 |

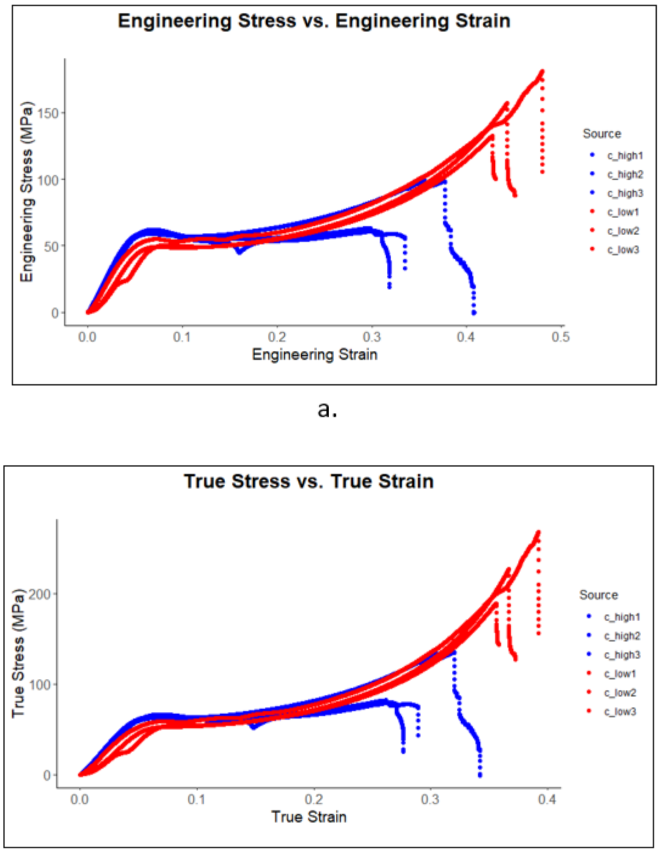

a.

b.

**Fig. 1. a. Compressive engineering stress and engineering train curve; b. Compressive true stress and true strain curve; strain rate of $10^{-3}$ $s^{-1}$ is marked with a blue graph; strain rate of $10^{-4}$ $s^{-1}$ is marked with a red graph**

The modulus of elasticity and yield stress values of the compressive test samples under different strain rates show results that the mechanical parameters tend to be different. The deviation values (δ) of the average Young's Modulus and average yield stress are 18.81% and 19.88%. These deviation values are obtained in this equation:

$$\delta_E = \frac{|\bar{E}_{high} - \bar{E}_{low}|}{\bar{E}_{low}} \times 100\% \quad dan \quad \delta_\sigma = \frac{|\bar{\sigma}_{high} - \bar{\sigma}_{low}|}{\bar{\sigma}_{low}} \times 100\% \quad (8)$$

The difference in the average value of modulus of elasticity and the average value of yield stress at a strain rate of $10^{-3}$ $s^{-1}$ and $10^{-4}$ $s^{-1}$ is shown in the table below:

**Tabel 2: The difference in the average value of elastic modulus and the average value of yield stress under varied strain rates**

| Strain rate ($s^{-1}$) | Average of Young's Modulus (GPa) | Average of Yield Stress (MPa) |
|---|---|---|
| $10^{-3}$ | 1.29 | 59.31 |
| $10^{-4}$ | 1.09 | 49.48 |
| **δ (%)** | **18.81** | **19.88** |

The standard deviation value for the modulus of elasticity of the three samples tested at a low strain rate ($10^{-4}$ $s^{-1}$) was 0.066 GPa; while that for the three samples tested at a high strain rate ($10^{-3}$ $s^{-1}$) was 0.043 GPa. Meanwhile, the standard deviation value for yield stress for the three samples tested with a low strain rate ($10^{-4}$ $s^{-1}$) was 1.633 MPa; while for the three samples tested with a high strain rate ($10^{-4}$ $s^{-1}$) was 0.633 MPa.

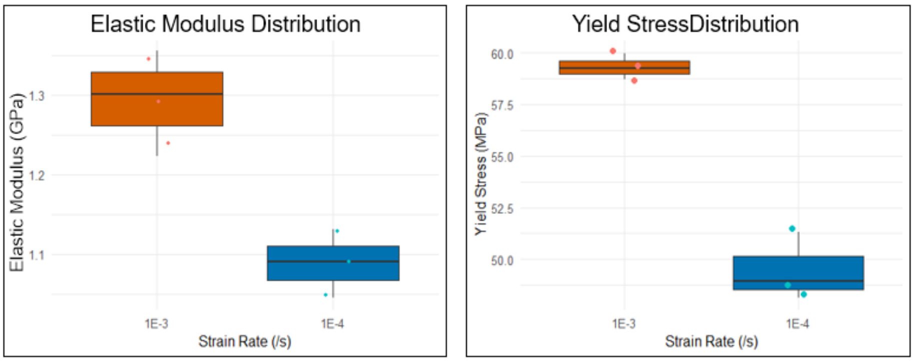

a.

b.

**Fig. 5. a Boxplot of the distribution of elastic modulus values; b. Boxplot of yield stress value distribution.**

To investigate whether the average values of Young's Modulus and yield stress at 10-3 /s and 10-4 /s are considered to have significant differences or not, a T-test hypothesis test was conducted. The T-test was conducted in R studio software.

The results of the T-test on the average value of Young's Modulus show that the p-value is 0.01116; this value is lower than the p-value threshold of 0.05; meaning that we reject the null hypothesis stating that there is no significant difference between the average groups.

The T-test results on the mean yield stress values show that the p-value is 0.00066; this value is lower than the p-value threshold of 0.05; meaning that we reject the null hypothesis stating that there is no significant difference between the group means. The conclusion is that there is a significant difference between the mean Young's Modulus and mean yield stress values tested at $10^{-4}s^{-1}$ and $10^{-3}$ $s^{-1}$ strain rates.

3.1.2 Tensile Test Result

The tests were conducted on 2 samples where the first samples were tested at a strain rate of $10^{-3}$ $s^{-1}$ while the second sample were tested at a strain rate of $10^{-4}$ $s^{-1}$. The test resulting the force and displacement information that can be processed into engineering stress and engineering strain curve, as well as true stress and true strain curve through the Eq. 2 and 3 respectively as shown in Fig. 6. Table 3 shows the difference result of Young's Modulus and yield stress between strain rate of $10^{-3}$ $s^{-1}$ and strain rate of $10^{-4}$ $s^{-1}$.

Poisson's Ratio measurement was done by comparing lateral strain and longitudinal strain. Samples were marked longitudinally and laterally first, then the markings were scanned by a Digital Image Correlation (DIC) device. The result shown in Fig. 7.

When the initial loading occurs or when the strain is low, the Poisson's Ratio value tends to be unstable. Until the strain reaches 0.02, the Poisson's Ratio value tends to stabilize around 0.4 until the elasticity limit. It can be concluded that the Poisson's Ratio value of the sample is 0.4.

**Tabel 3: Extraction of tensile test parameters**

| Label | Strain Rate | Modulus Young (GPa) | Tensile Yield Stress (MPa) |
|---|---|---|---|
| t_high | 10-3 s-1 | 0.99 | 31.20 |
| t_low | 10-4 s-1 | 0.90 | 21.69 |
| | **δ (%)** | **9.76** | **43.82** |

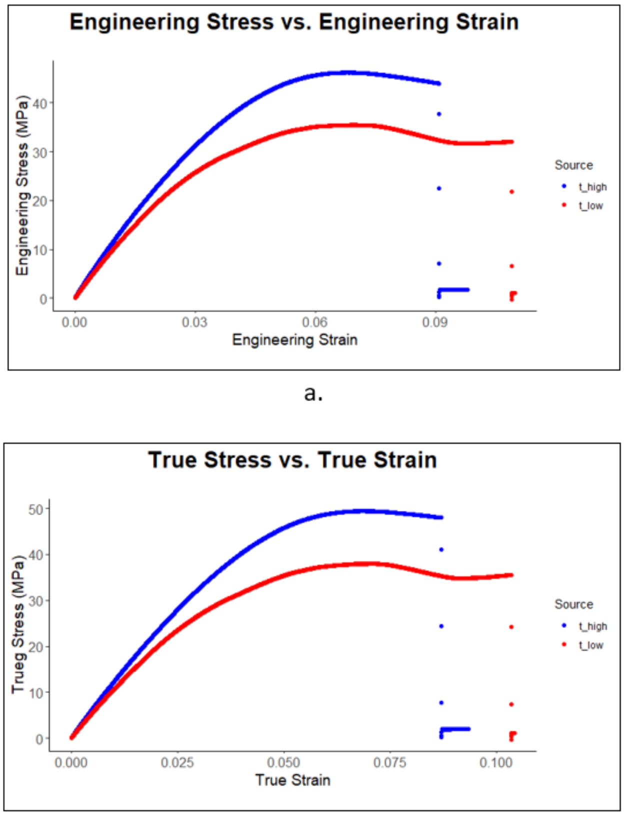

a.

b.

**Figure 6. a. Tensile engineering stress and engineering train curve; b. Tensile true stress and true strain curve; strain rate of $10^{-3}$ $s^{-1}$ is marked with a blue graph; strain rate of $10^{-4}$ $s^{-1}$ is marked with a red graph**

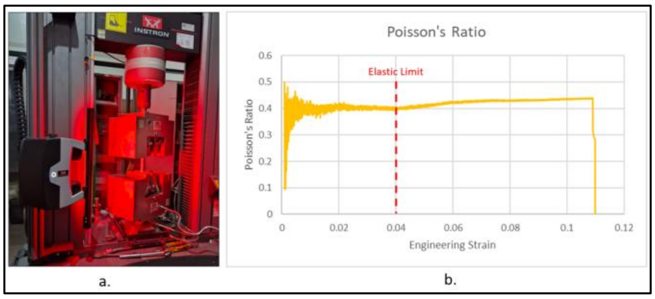

**Fig.7. a. Tensile test process with DIC; b. Poisson's ratio graph along strain curve**

### 3.2 Simplified Zhu – Wang – Tang Constitutive Model

The first curve fitting process was done by matching between $\Delta\sigma$ from Eq. 5 and the function from Eq. 6. This step was used to determine the $E_1$ and $\theta_1$ of PLA sample. The first curve fitting process is shown in Fig. 8a. The variables obtained from the first curve fitting process are $E_1$ = 1847.045 MPa and $\theta_1$ = 9.15 s. The second curve fitting process was done by matching one of the experimental test result and the function from Eq. 4 with the value of $E_1$ and $\theta_1$ from the first curve fitting process. The second curve fitting process is shown in Fig. 8b. The variables obtained from the second curve fitting process are $E_0$ = - 0.288 GPa; $\alpha$ = 54.751 GPa; and $\beta$ = -631.187 GPa.

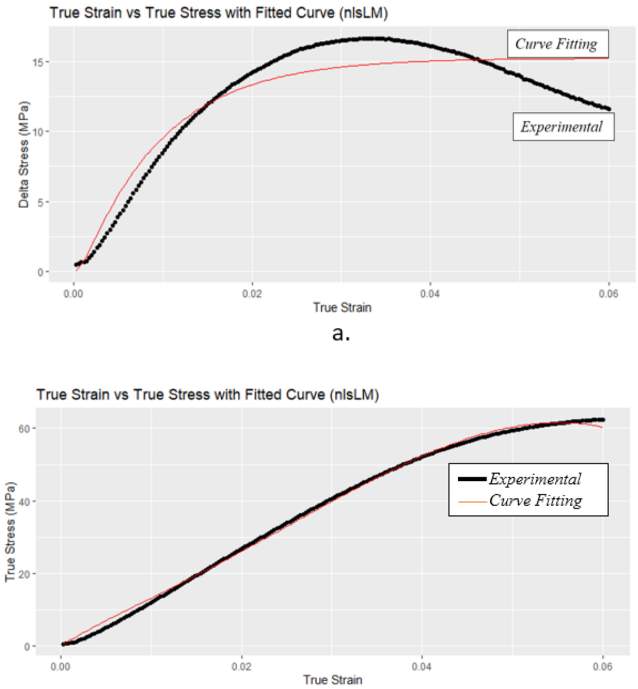

a.

b.

**Fig. 8. a. The first curve fitting to find $E_1$ and $\theta_1$; b. The second curve fitting to find $E_0$, $\alpha$, and $\beta$.**

The final form of the Simplified ZWT equation of PLA through SLA 3D printing fabrication method is as follows:

$$\sigma = -0{,}288\varepsilon + 54{,}751\varepsilon^2 - 631{,}187\varepsilon^3 + 1{,}847\int_0^t \dot{\varepsilon} exp\left(-\frac{t-\tau}{9{,}15}\right)d\tau \quad (9)$$

The validation of this simplified ZWT constitutive model was done by comparing the constitutive model with the true stress and true strain curves from compressive testing results with strain rates of $10^{-3}$ $s^{-1}$ and $10^{-4}$ $s^{-1}$. The validation process of the constitutive model was considered through the statistical parameter $R^2$.

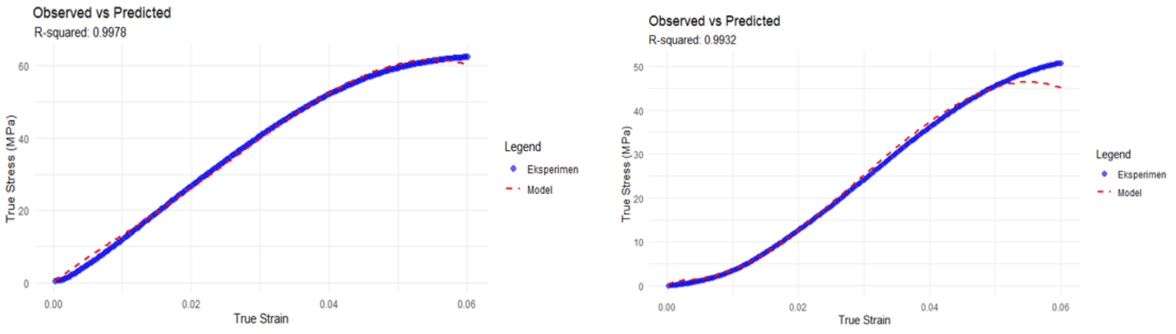

a.

b.

**Fig. 9. a. Validation process of compressive testing data with a strain rate $10^{-3}$ $s^{-1}$ with the Simplified ZWT Constitutive Model; b. Validation process of compressive testing data with a strain rate $10^{-4}$ $s^{-1}$ with the Simplified ZWT Constitutive Model**

Based on the calculation, the $R^2$ value in the comparison of compressive testing data with a strain rate $10^{-3}$ $s^{-1}$ with the Simplified ZWT Constitutive Model is 0.9978. In addition, the $R^2$ value in the comparison of compressive test data with $10^{-4}$ $s^{-1}$ with the Simplified ZWT Constitutive Model is 0.9932. Since both of $R^2$ value are greater than 0.9, it can be concluded that the constitutive model is valid to describe the mechanical behavior of PLA through SLA 3D printing fabrication method.

### 3.3 Mohr – Coulomb Failure Criterion

The compression and tension test result shows that both Young's Modulus and yield stress values have the significant difference of values. Table 4 shows a comparison of compressive and tensile tests tested with a variation of the $10^{-3}$ $s^{-1}$ and $10^{-4}$ $s^{-1}$ strain rate.

The data that we used for modeling the Mohr - Coulomb failure criterion of PLA is tensile and compressive testing data at a strain rate of $10^{-4}$ $s^{-1}$. This is because the yield strength values of both compressive and tensile at these strain rates show lower results. The failure model with lower yield strength indicates safer failure criteria under more common loading conditions.

**Tabel 4: Comparison of compression and tension experiment result**

| $\dot{\varepsilon}$ ($s^{-1}$) | E (GPa) | | **δ (%)** | $\sigma_y$ (MPa) | | **δ (%)** |
|---|---|---|---|---|---|---|
| | C | T | | C | T | |
| $10^{-3}$ | 1.29 | 0.99 | **30.30** | 59.31 | 31.20 | **90.10** |
| $10^{-4}$ | 1.09 | 0.90 | **21.11** | 49.48 | 21.69 | **128.12** |

Note: C – Compression test result
T – Tension test result

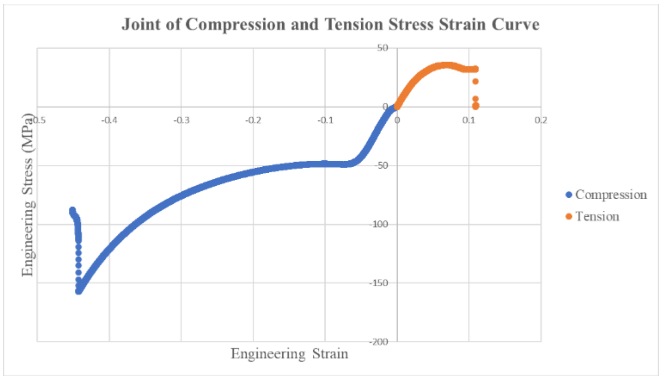

**Fig. 10. Comparison of compression and tension test result in stress strain curve**

From the tension test, the tensile yield strength $\sigma_{y.t}$ is 21.69 MPa, while the compressive yield strength $\sigma_{y.c}$ is 49.48 MPa. We can model this situation through Mohr's circle as shown at Fig. 11.

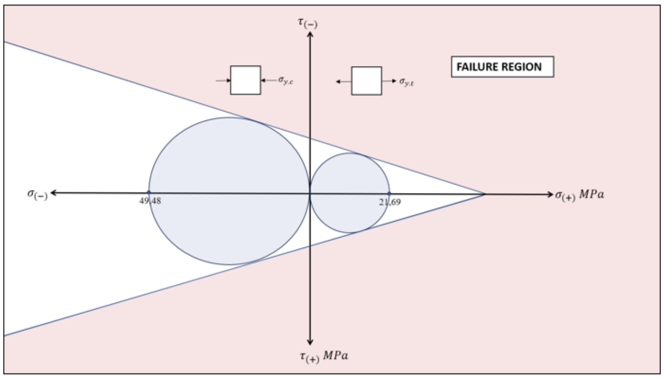

**Fig. 11. Mohr circle analysis of PLA’s Mohr - Coulomb failure criteria**

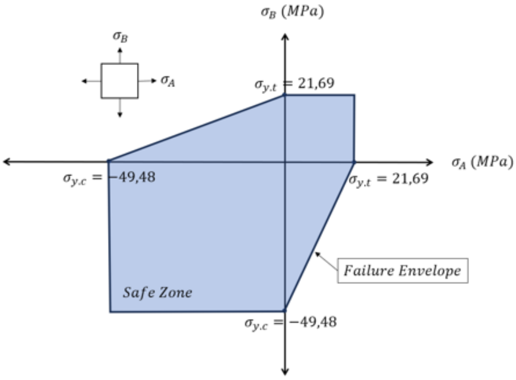

**Fig. 12. Plane Stress Yield Surface of PLA**

The mathematical equation for the failure limit of PLA's Mohr - Coulomb failure model is as follows:

$$\frac{\sigma_1}{21{,}69\,MPa} - \frac{\sigma_3}{49{,}48\,MPa} \leq 1 \quad (10)$$

## 4. Conclusion

The results of compressive and tensile testing of PLA samples through the SLA 3D printing fabrication method at different strain rates show significant differences in values. Young's Modulus and Yield Stress values at lower strain rates showed lower values. The simplified ZWT constitutive model (Eq. 9) of PLA is considered as a valid model under varied strain rates. The Mohr – Coulomb failure criteria model (Eq. 10) can describe the failure region of PLA under the variation of loadings.

**Author Contributions:** Fabrication of samples, B.D.; writing – original draft preparation, B.D.; writing – review and editing, B.B., M.A.K., A.W.; supervision, , B.B., M.A.K., A.W.

**Acknowledgements:** We would like to acknowledge LPDP and BPPT for the contribution towards my doctoral study and research funding.

## References

[1] Cloete, T.J., Paul, G., Ismail, E.B., 2014. Hopkinson bar techniques for the intermediate strain rate testing of bovine cortical bone, in: Philosophical Transactions of the Royal Society A: Mathematical, Physical and Engineering Sciences. Royal Society of London. https://doi.org/10.1098/rsta.2013.0210

[2] DeStefano, V., Khan, S., Tabada, A., 2020. Applications of PLA in modern medicine. Engineered Regeneration 1, 76–87. https://doi.org/10.1016/j.engreg.2020.08.002

[3] Esmaeili, S., Akbari Aghdam, H., Motififard, M., Saber-Samandari, S., Montazeran, A.H., Bigonah, M., Sheikhbahaei, E., Khandan, A., 2020. A porous polymeric–hydroxyapatite scaffold used for femur fractures treatment: fabrication, analysis, and simulation. European Journal of Orthopaedic Surgery and Traumatology 30, 123–131. https://doi.org/10.1007/s00590-019-02530-3

[4] Gao, G., Tang, E., Yang, G., Han, Y., Chuangchen, Chang, M., Guo, K., He, L., 2024. Parameter determination and verification of ZWT viscoelastic dynamic constitutive model of Al/Ep/W material considering strain rate effect. Int J Impact Eng 184, 104816. https://doi.org/10.1016/j.ijimpeng.2023.104816

[5] Gide, K.M., Islam, S., Bagheri, Z.S., 2022. Polymer-Based Materials Built with Additive Manufacturing Methods for Orthopedic Applications: A Review. Journal of Composites Science. https://doi.org/10.3390/jcs6090262

[6] Han, X., Yang, D., Yang, C., Spintzyk, S., Scheideler, L., Li, P., Li, D., Geis-Gerstorfer, J., Rupp, F., 2019. Carbon fiber reinforced PEEK composites based on 3D-printing technology for orthopedic and dental applications. J Clin Med 8. https://doi.org/10.3390/jcm8020240

[7] Hassanajili, S., Karami-Pour, A., Oryan, A., Talaei-Khozani, T., 2019. Preparation and characterization of PLA/PCL/HA composite scaffolds using indirect 3D printing for bone tissue engineering. Materials Science and Engineering C 104. https://doi.org/10.1016/j.msec.2019.109960

[8] Islam, M.S., Abdulla-Al-Mamun, M., Khan, A., Todo, M., 2020. Excellency of Hydroxyapatite Composite Scaffolds for Bone Tissue Engineering.

[9] Ji, Q., Wang, Z., Yi, J., Tang, X., 2021. Mechanical properties and a constitutive model of 3d-printed copper powder-filled pla material. Polymers (Basel) 13. https://doi.org/10.3390/polym13203605

[10] Ma, R., Tang, T., 2014. Current strategies to improve the bioactivity of PEEK. Int J Mol Sci. https://doi.org/10.3390/ijms15045426

[11] Niaounakis, M., 2015. Biopolymers: Applications and trends, Biopolymers: Applications and Trends.

[12] Prot, M., Cloete, T.J., Saletti, D., Laporte, S., 2016. The behavior of cancellous bone from quasi-static to dynamic strain rates with emphasis on the intermediate regime. J Biomech 49, 1050–1057. https://doi.org/10.1016/j.jbiomech.2016.02.021

[13] Raffa, M.L., Nguyen, V.H., Hernigou, P., Flouzat-Lachaniette, C.H., Haiat, G., 2021. Stress shielding at the bone-implant interface: Influence of surface roughness and of the bone-implant contact ratio. Journal of Orthopaedic Research 39, 1174–1183. https://doi.org/10.1002/jor.24840

[14] Ranjan, N., Singh, R., Ahuja, I.P.S., Kumar, R., Singh, J., Verma, A.K., Leekha, A., 2020. On 3D printed scaffolds for orthopedic tissue engineering applications. SN Appl Sci 2. https://doi.org/10.1007/s42452-020-1936-8

[15] Sælen, R.L., Hopperstad, O.S., Clausen, A.H., 2023. Mechanical behaviour and constitutive modelling of an additively manufactured stereolithography polymer. Mechanics of Materials 185. https://doi.org/10.1016/j.mechmat.2023.104777

[16] Sreekumar, K., Bindhu, B., Veluraja, K., 2021. Perspectives of polylactic acid from structure to applications. Polymers from Renewable Resources. https://doi.org/10.1177/20412479211008773

[17] Wang, W., Zhang, B., Li, M., Li, J., Zhang, C., Han, Y., Wang, L., Wang, K., Zhou, C., Liu, L., Fan, Y., Zhang, X., 2021. 3D printing of PLA/n-HA composite scaffolds with customized mechanical properties and biological functions for bone tissue engineering. Compos B Eng 224. https://doi.org/10.1016/j.compositesb.2021.109192

[18] Wu, D., Spanou, A., Diez-Escudero, A., Persson, C., 2020. 3D-printed PLA/HA composite structures as synthetic trabecular bone: A feasibility study using fused deposition modeling. J Mech Behav Biomed Mater 103. https://doi.org/10.1016/j.jmbbm.2019.103608

[19] Xu, X., Gao, S., Ou, Z., Ye, H., 2018. Mechanical behavior of liquid nitrile rubber-modified epoxy resin under static and dynamic loadings: Experimental and constitutive analysis. Materials 11. https://doi.org/10.3390/ma11091565

[20] Zhang, B., Wang, L., Song, P., Pei, X., Sun, H., Wu, L., Zhou, C., Wang, K., Fan, Y., Zhang, X., 2021. 3D printed bone tissue regenerative PLA/HA scaffolds with comprehensive performance optimizations. Mater Des 201. https://doi.org/10.1016/j.matdes.2021.109490

[21] Zhou, C., Liu, L., Wang, W., Zhao, L., Li, M., Li, J., Zhang, B., Han, Y., Wang, L., Zhang, Z., 2021. Fabrication and properties of PLA/nano-HA composite scaffolds with balanced mechanical properties and biological functions for bone tissue engineering application. Nanotechnol Rev 10, 1359–1373. https://doi.org/10.1515/ntrev-2021-0083

[22] Zimmermann, E.A., Gludovatz, B., Schaible, E., Busse, B., Ritchie, R.O., 2014. Fracture resistance of human cortical bone across multiple length-scales at physiological strain rates. Biomaterials 35, 5472–5481. https://doi.org/10.1016/j.biomaterials.2014.03.066.